Electronic Supplementary Information

A Simple, Rapid and Scalable Synthesis Approach for Ultra-Small Size Transition Metal Selenides with Efficient Water Oxidation Performance

*Yue Shi,[a, +] Dan Zhang,[a, b, +] Hongfu Miao,[a] Wen Zhang,[a] Xueke Wu,[a] Zuochao Wang,[a] Hongdong Li,[a] Tianrong Zhan,[a] Xilei Chen,[b] Jianping Lai[a] * and Lei Wang[a, b] **

[a] *Key Laboratory of Eco-chemical Engineering, Key Laboratory of Optic-electric Sensing and Analytical Chemistry of Life Science, Taishan Scholar Advantage and Characteristic Discipline Team of Eco Chemical Process and Technology, College of Chemistry and Molecular Engineering, Qingdao University of Science and Technology, Qingdao, P. R. China.*

Corresponding author: inorchemwl@126.com (L. Wang); jplai@qust.edu.cn (J. Lai)

[b] *Shandong Engineering Research Center for Marine Environment Corrosion and Safety Protection, College of Environment and Safety Engineering, Qingdao University of Science and Technology, Qingdao 266042, P. R. China*

[+] *These authors contributed equally to this work.*

Experimental section:

Chemicals. Nickel (II) acetate tetrahydrate ($(CH_3COO)_2Ni·4H_2O$, 99%, Aladdin), cobalt (II) acetate tetrahydrate ($(CH_3COO)_2Co·4H_2O$, 99.5%, Macklin), ferrocene ($Fe(C_5H_5)_2$, 99%, Aladdin), selenium (Se, >99.99%, Aladdin), carboxylated multi-walled carbon nanotube (CNT, >95%, Aladdin), potassium hydroxide (KOH, 90%, Aladdin), Nafion solution (5%, Sigma-Aldrich), ethanol (C_2H_6O, >99.8%, Sinopharm Chemical Reagent Co., Ltd.). The deionized water used in all experiments was ultrapure water (18.2 MΩ·cm).

Preparation of $Ni_{0.85}Se$@CNT. $(CH_3COO)_2Ni·4H_2O$ (10 mg), Se powder (10 mg) and CNT (10 mg) were well mixed using the mortar. Afterwards, the homogeneous mixture was placed in a quartz vial and argon gas was injected into quartz vial until full filled. The quartz vial was then placed in a domestic microwave oven and heated at 700 W for 120 seconds. Subsequently, the quartz vial was cooled naturally to room temperature. At last, the obtained black powder was washed twice with deionized water and twice with ethanol, and then collected by centrifugation.

Preparation of $Ni_{0.41}Fe_{0.44}Se$@CNT. $(CH_3COO)_2Ni·4H_2O$ (5 mg), $Fe(C_5H_5)_2$ (5 mg), Se powder (10 mg) and CNT (10 mg) were well mixed using the mortar. Other steps are exactly the same as $Ni_{0.85}Se$@CNT.

Preparation of $Co_{0.42}Fe_{0.43}Se$@CNT. $(CH_3COO)_2Co·4H_2O$ (5 mg), $Fe(C_5H_5)_2$ (5 mg), Se powder (10 mg) and CNT (10 mg) were well mixed using the mortar. Other steps are exactly the same as $Ni_{0.85}Se$@CNT.

Preparation of $Ni_{0.27}Co_{0.28}Fe_{0.30}Se$@CNT. $(CH_3COO)_2Ni·4H_2O$ (3 mg), $(CH_3COO)_2Co·4H_2O$ (3 mg), $Fe(C_5H_5)_2$ (3 mg), Se powder (10 mg) and CNT (10 mg) were well mixed using the mortar. Other steps are exactly the same as $Ni_{0.85}Se$@CNT.

Preparation of $Ni_{0.33}Co_{0.32}Fe_{0.35}$@CNT. $(CH_3COO)_2Ni·4H_2O$ (3 mg), $(CH_3COO)_2Co·4H_2O$ (3 mg), $Fe(C_5H_5)_2$ (3 mg) and CNT (5 mg) were well mixed using the mortar. Other steps are exactly the same as $Ni_{0.85}Se$@CNT.

Preparation of NiCoFeSe@CNT in different NiCoFe:Se proportions. $(CH_3COO)_2Ni·4H_2O$ (3 mg), $(CH_3COO)_2Co·4H_2O$ (3 mg), $Fe(C_5H_5)_2$ (3 mg), CNT (10 mg) and Se powder (10 mg) for NiCoFe:Se = 1:1, $(CH_3COO)_2Ni·4H_2O$ (3 mg), $(CH_3COO)_2Co·4H_2O$ (3 mg), $Fe(C_5H_5)_2$ (3 mg), CNT (10 mg) and Se powder (5 mg) for NiCoFe:Se = 2:1 and $(CH_3COO)_2Ni·4H_2O$ (3 mg), $(CH_3COO)_2Co·4H_2O$ (3 mg), $Fe(C_5H_5)_2$ (3 mg), CNT (10 mg) and Se powder (20 mg) for NiCoFe:Se = 1:2. Other steps are exactly the same as $Ni_{0.85}Se$@CNT.

Characterization. Powder X-ray diffraction (XRD) patterns were recorded on a X'Pert-Pro MPD diffractometer with Cu Kα radiation at 40 KV and 40 mA. Scanning electron microscopy (SEM) images were obtained by Hitachi, S-8200. The transmission electron microscope (TEM) and high resolution TEM (HRTEM) of the catalyst were tested using FEI Tecnai-G2 F30 at an accelerating voltage of 300 KV. X-ray photoelectron spectroscopy (XPS) analysis was performed with an Axis Supra spectrometer using a monochromatic Al Kα source at 15 mA and 14 kV. Scan analysis with an analysis area of 300 × 700 microns and a pass energy of 100 eV. The XPS spectra were calibrated by carbon 1 s spectrum, and its main line was set to 284.6 eV. The catalysts after the durability tests were sonicated in ethanol and collected for further characterization.

Electrochemical measurements. The electrochemical measurements were carried out on CHI 660 electrochemical workstation (CH Instruments, Inc., Shanghai) with a typical three-electrode system. The reference electrode and counter electrode were Ag/AgCl reference electrode and Pt foil, respectively. The working electrode was a glassy carbon electrode (GCE, diameter: 3 mm, area: 0.07065 cm^2). The potentials were converted to the reversible hydrogen electrode (RHE) according to the Nernst equation: E (RHE) = E (Ag/AgCl) + 0.199 V + 0.059 × pH. The catalysts were dispersed in ethanol+5% Nafion mixed solution (v:v=100:1) and then sonicated for 1 h to obtain homogeneous catalyst ink with concentration of 5 mg/mL. Subsequently, 10 μL of the catalyst ink was dropped onto the surface of the GCE for further electrochemical tests. The OER performance and durability test were evaluated in O_2-saturated 1.0 M KOH solution. And all the measurements were carried out at room temperture. Typical OER polarization curves were obtained through a linear sweep voltammetry (LSV) measurements with a scan rate of 5 mV s^{-1} and corrected for iR compensation level of 95%. The overpotential (η) is calculated by subtracting 1.23 V which is the theoretical potential for oxygen evolution *vs* RHE from the iR-corrected E (*vs* RHE). Electrochemical impedance spectroscopy (EIS) were measured at 0.45V *vs.* Ag/AgCl in the frequency range from 10 kHz to 0.01 Hz in O_2-saturated 1.0 M KOH solution. The electrochemically active surface area (ECSA) was calculated by electrochemical double-layer capacitance (C_{dl}) method. To derive the C_{dl}, the following equation was used: $C_{dl} = I_c/\nu$, where C_{dl} was the double-layer capacitance (mF cm^{-2}) of the electroactive materials, I_c was charging current (mA cm^{-2}) and ν was scan rate (mV s^{-1}). The ECSA was calculated from the double layer capacitance according to the following equation: $ECSA = \frac{C_{dl} \times S}{C_s}$, where C_s was the specific capacitance (0.040 mF cm^{-2}), S was the geometric surface area of electrode (0.07065 cm^2). The number of active sites (n) was calculated by

the following formula: $n = \frac{ECSA \times M \times N_0}{N_A}$. M is the mass loading of catalyst on the electrode, N_0 is the constant of metal surface concentration (Fe =1.63*1019/m^2, Co=1.51*1019/m^2, Ni =1.54*1019/ m^2) and N_A is the Avogadro constant. The the turnover frequency (TOF) values were calculated from the following equation: $TOF = \frac{j}{4 * F * n}$. Here, j is the current (A) during linear sweep voltammetry (LSV) with 95% iR-corrected, F is the Faraday constant (F=96485.3 C mol^{-1}), n is the number of active sites (mol). The factor 1/4 is due to the forming of oxygen as a four-electron process.

Supplementary Figures.

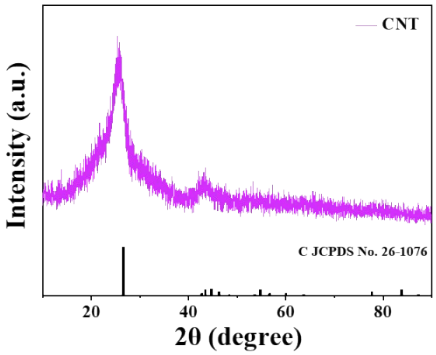

Fig. S1 XRD pattern of CNT.

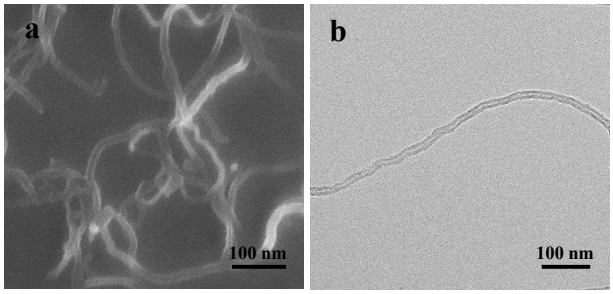

Fig. S2 (a) SEM image and (b) TEM image of CNT.

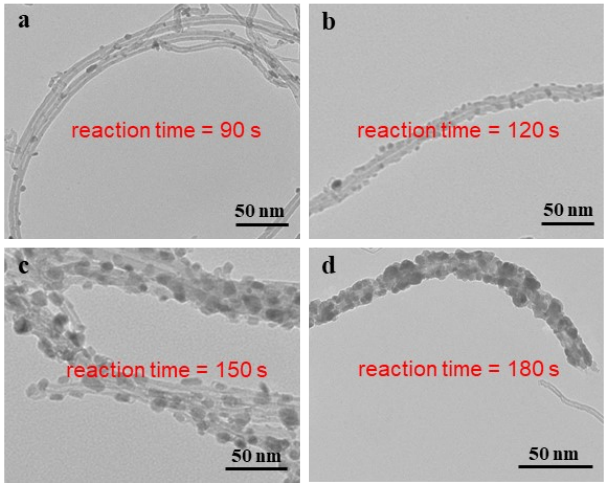

Fig. S3 TEM images of $Ni_{0.27}Co_{0.28}Fe_{0.30}Se$@CNT with different reaction times.

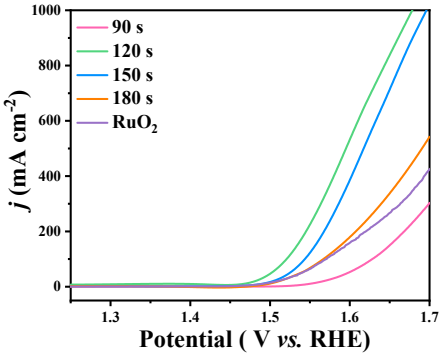

Fig. S4 OER polarization curves of $Ni_{0.27}Co_{0.28}Fe_{0.30}Se$@CNT with different reaction times.

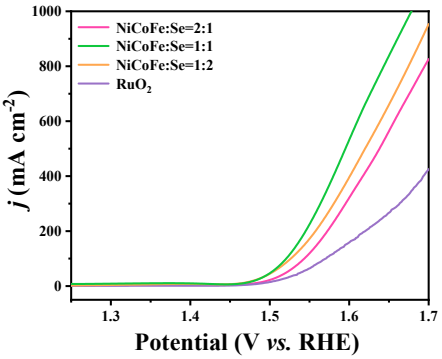

Fig. S5 LSV curves of NiCoFeSe@CNT with different feeding ratios in 1.0 M KOH.

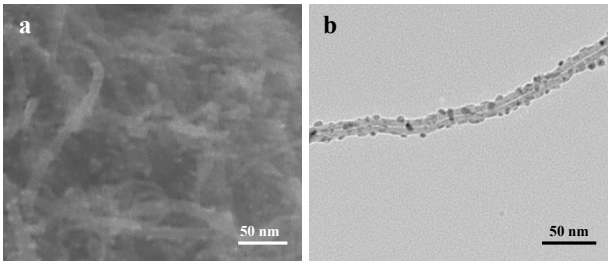

Fig. S6 (a) SEM image and (b) TEM image of $Ni_{0.27}Co_{0.28}Fe_{0.30}Se$@CNT.

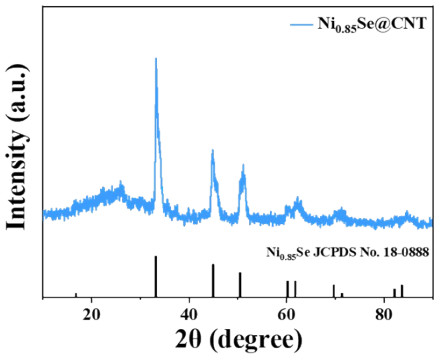

Fig. S7 XRD pattern of $Ni_{0.85}Se$@CNT.

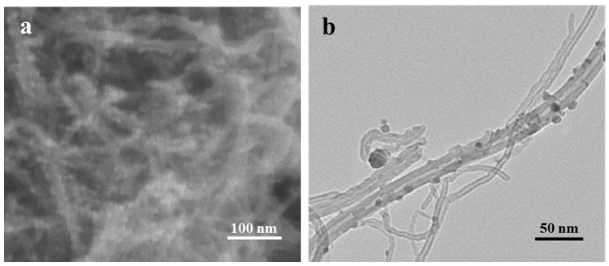

Fig. S8 (a) SEM image and (b) TEM image of $Ni_{0.85}Se$@CNT.

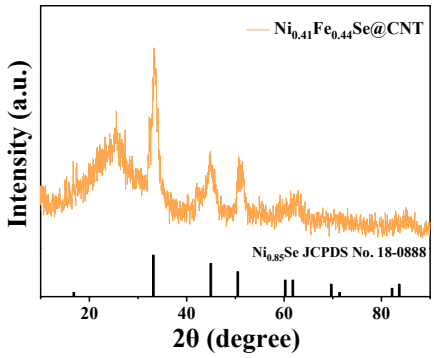

Fig. S9 XRD pattern of $Ni_{0.41}Fe_{0.44}Se$@CNT.

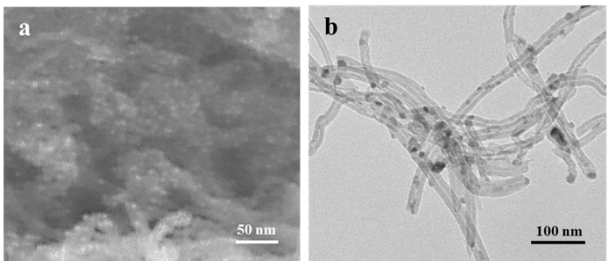

Fig. S10 (a) SEM image and (b) TEM image of $Ni_{0.41}Fe_{0.44}Se$@CNT.

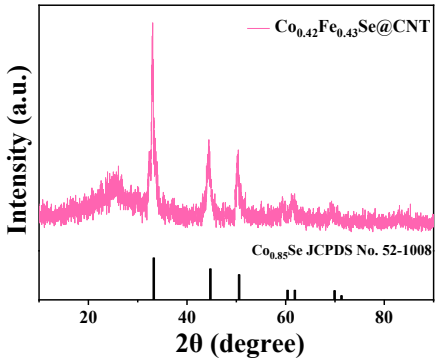

Fig. S11 XRD pattern of $Co_{0.42}Fe_{0.43}Se$@CNT.

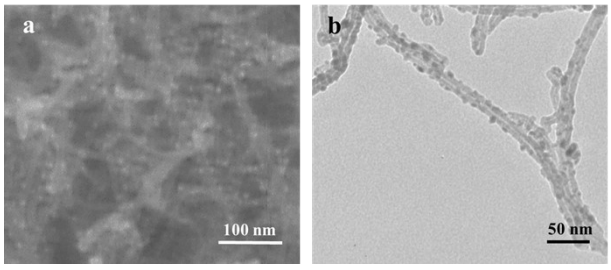

Fig. S12 (a) SEM image and (b) TEM image of $Co_{0.42}Fe_{0.43}Se$@CNT.

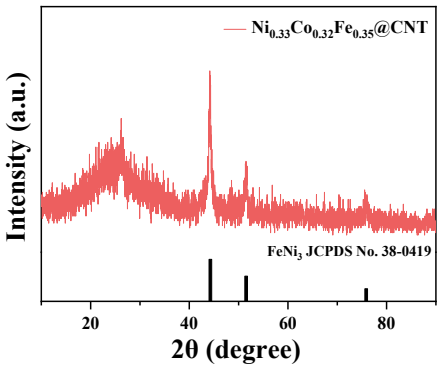

Fig. S13 XRD pattern of $Ni_{0.33}Co_{0.32}Fe_{0.35}$@CNT.

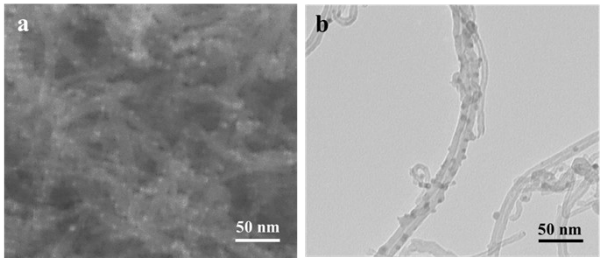

Fig. S14 (a) SEM image and (b) TEM image of $Ni_{0.33}Co_{0.32}Fe_{0.35}$@CNT.

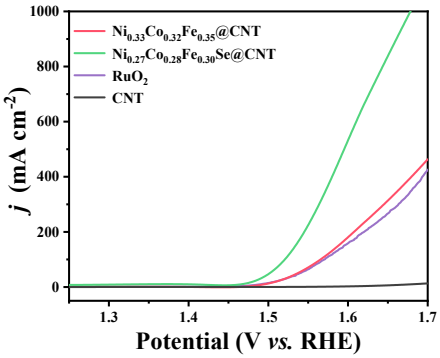

Fig. S15 LSV curves of $Ni_{0.33}Co_{0.32}Fe_{0.35}$@CNT, $Ni_{0.27}Co_{0.28}Fe_{0.30}Se$@CNT, the commercial RuO_2 and CNT.

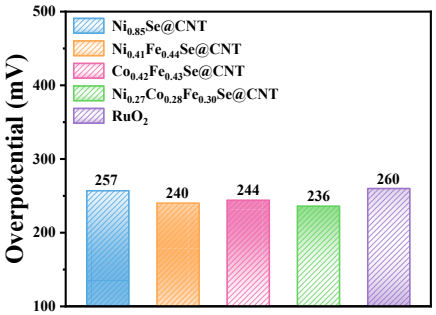

Fig. S16 Overpotentials of different electrocatalysts at the current density of 10 mA cm^{-2}.

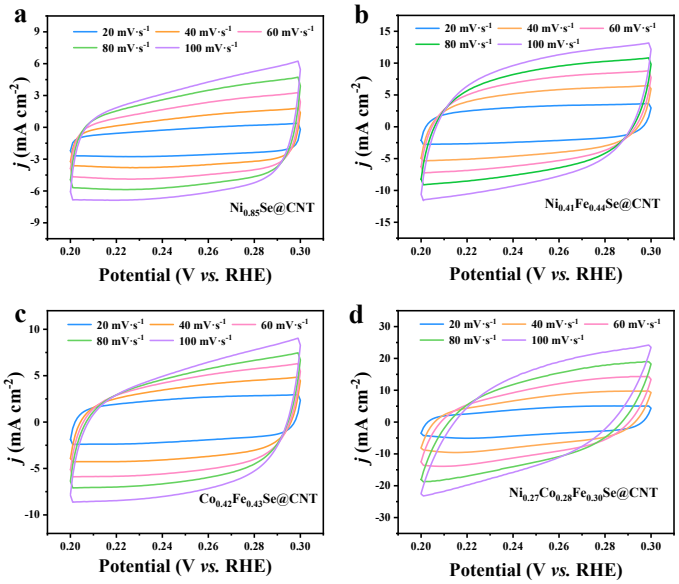

Fig. S17 CV curves measured at different scan rates from 20 to 100 mV s^{-1} for (a) $Ni_{0.85}Se$@CNT, (b) $Ni_{0.41}Fe_{0.44}Se$@CNT, (c) $Co_{0.42}Fe_{0.43}Se$@CNT and (d) $Ni_{0.27}Co_{0.28}Fe_{0.30}Se$@CNT in 1.0 M KOH.

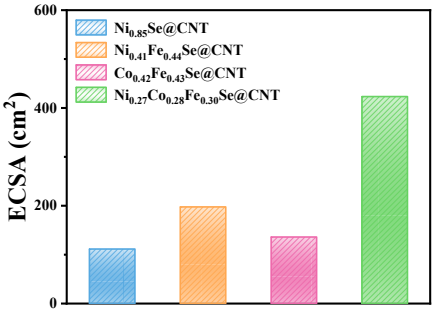

Fig. S18 Electrochemical surface areas of $Ni_{0.85}Se$@CNT, $Ni_{0.41}Fe_{0.44}Se$@CNT, $Co_{0.42}Fe_{0.43}Se$@CNT and $Ni_{0.27}Co_{0.28}Fe_{0.30}Se$@CNT.

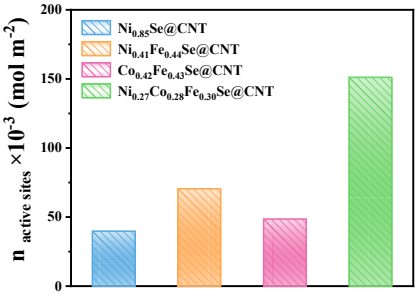

Fig. S19 The number of active sites in $Ni_{0.85}Se$@CNT, $Ni_{0.41}Fe_{0.44}Se$@CNT, $Co_{0.42}Fe_{0.43}Se$@CNT and $Ni_{0.27}Co_{0.28}Fe_{0.30}Se$@CNT.

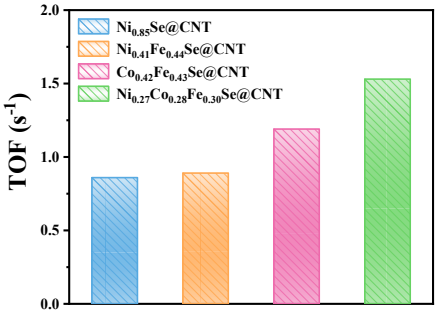

Fig. S20 TOF values of $Ni_{0.85}Se$@CNT, $Ni_{0.41}Fe_{0.44}Se$@CNT, $Co_{0.42}Fe_{0.43}Se$@CNT and $Ni_{0.27}Co_{0.28}Fe_{0.30}Se$@CNT at the overpotential of 500 mV.

Fig. S21 Photograph of catalyst yield after increasing the amount of reactants.

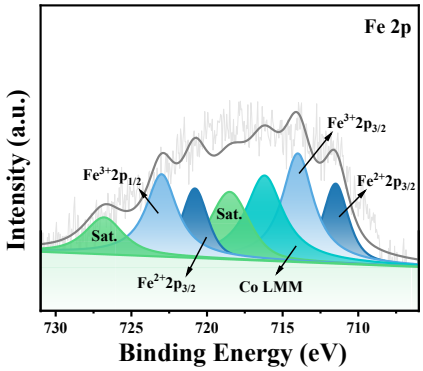

Fig. S22 XPS spectrum of Fe 2p in $Ni_{0.27}Co_{0.28}Fe_{0.30}Se$@CNT after stability test.

Tables

Table S1. Different atomic ratios in NiCoFeSe@CNT with different feeding ratios determined by XPS results.

	Ni (atom %)	Co (atom %)	Fe (atom %)	Se (atom %)
NiCoFe:Se=2:1	14	17	16	53
NiCoFe:Se=1:1	15	15	16	54
NiCoFe:Se=1:2	14	15	15	56

Table S2. Different atomic ratios of different catalysts determined by XPS results.

	Ni (atom %)	Co (atom %)	Fe (atom %)	Se (atom %)
$Ni_{0.85}Se$@CNT	46	—	—	54
$Ni_{0.41}Fe_{0.44}Se$@CNT	22	—	24	54
$Co_{0.42}Fe_{0.43}Se$@CNT	—	23	23	54
$Ni_{0.27}Co_{0.28}Fe_{0.30}Se$@CNT	15	15	16	54
$Ni_{0.33}Co_{0.32}Fe_{0.35}$@CNT	33	32	35	—

Table S3. OER performance comparison of recently reported transition metal-based catalysts.

Catalysts	Overpotential (mV @ mA cm^{-2})	Tafel Slope (mV dec^{-1})	ECSA (cm^{-2})	TOF (s^{-1} @ mV)	Electrolyte	Ref.
$Ni_{0.27}Co_{0.28}Fe_{0.30}Se$@CNT	236 @ 10 291 @ 100 365 @ 500	44.1	423.4	1.53 @ 500	1.0 M KOH	This Work
$Ni_{0.83}Fe_{0.17}(OH)_2$	245 @ 10 300 @ 41	61	37.3	N/A	1.0 M KOH	[1]

NiFe-MOF/G	258 @ 10 340 @ 100	49	26.5	1.80 @ 350	1.0 M KOH	[2]
defect-rich porous monolayer NiFe-LDH	230 @ 10 340 @ 100	47	3.7	N/A	0.1 M KOH	[3]
hierarchical Ni–Fe LDH nanocages	246 @ 20 272 @ 50	71	5.5	N/A	1.0 M KOH	[4]
Fe_1Co_1-oxide nanosheets	308 @ 10	36.8	24.9	0.022 @ 350	0.1 M KOH	[5]
amorphous NiFeMo oxide	280 @ 10	49	0.74	N/A	0.1 M KOH	[6]
single-unit-cell thick $CoSe_2$	270 @ 10 470 @ 73	64	0.073	0.21 @ 470	1.0 M KOH	[7]
Ag-$CoSe_2$ nanobelts	320 @ 10 350 @ 22.4	56	26.5	N/A	0.1 M KOH	[8]
NiFeMn-LDH	289 @ 20 320 @ 100	47	65.1	0.0038 @ 500	1.0 M KOH	[9]
Co-C@NiFe LDH	249 @ 10 328 @ 100	57.9	30.8	0.0223 @ 300	1.0 M KOH	[10]
Fe-doped $CoSe_2$@N-CNT	330 @ 10	74	144.1	N/A	1.0 M KOH	[11]
NiFe-LDH/CNT	250 @ 5	31	N/A	0.56 @ 300	1.0 M KOH	[12]
Fe-incorporated a-$Co(OH)_2$	295 @10 350 @ 100	52	91.3	0.027 @ 300	1.0 M KOH	[13]
Ni_1Fe_2 nanofoams	190 @ 10 291 @ 100	70	1.66	0.162 @ 300	1.0 M KOH	[14]
Fe–Ni_2P@PC/Cu_xS	330 @ 50 390 @ 100	140	75.2	N/A	1.0 M KOH	[15]
amorphous NiFe alloy	242 @ 10	24	0.25	N/A	1.0 M KOH	[16]
NiFeP/MXene	286 @ 10	35	19	0.35 @ 300	1.0 M KOH	[17]

Reference

1. Q. Zhou, Y. Chen, G. Zhao, Y. Lin, Z. Yu, X. Xu, X. Wang, H. K. Liu, W. Sun and S. X. Dou, *ACS Catal.*, 2018, **8**, 5382-5390.
2. Y. Wang, B. Liu, X. Shen, H. Arandiyan, T. Zhao, Y. Li, M. Garbrecht, Z. Su, L. Han, A. Tricoli and C. Zhao, *Adv. Energy Mater.*, 2021, **11**, 2003759.
3. X. Zhang, Y. Zhao, Y. Zhao, R. Shi, G. I. N. Waterhouse and T. Zhang, *Adv. Energy Mater.*, 2019, **9**, 1900881.
4. J. Zhang, L. Yu, Y. Chen, X. F. Lu, S. Gao and X. W. Lou, *Adv. Mater.*, 2020, **32**, 1906432.
5. L. Zhuang, L. Ge, Y. Yang, M. Li, Y. Jia, X. Yao and Z. Zhu, *Adv. Mater.*, 2017, **29**, 1606793.
6. S.-H. Yu, Y. Duan, Z.-Y. Yu, S.-j. Hu, X.-S. Zheng, C.-T. Zhang, H.-H. Ding, B.-C. Hu, Q.-Q. Fu, Z.-L. Yu, X. Zheng, J.-F. Zhu and M.-R. Gao, *Angew. Chem. Int. Ed.*, 2019, **58**, 15772-15777.
7. L. Liang, H. Cheng, F. Lei, J. Han, S. Gao, C. Wang, Y. Sun, S. Qamar, S. Wei and Y. Xie, *Angew. Chem. Int. Ed.*, 2015, **54**, 12004-12008.
8. X. Zhao, H. Zhang, Y. Yan, J. Cao, X. Li, S. Zhou, Z. Peng and J. Zeng, *Angew. Chem. Int. Ed.*, 2017, **56**, 328-332.
9. Z. Lu, L. Qian, Y. Tian, Y. Li, X. Sun and X. Duan, *Chem. Commun.*, 2016, **52**, 908-911.
10. W. Li, S. Chen, M. Zhong, C. Wang and X. Lu, *Chem. Eng. J*, 2021, **415**, 128879.
11. J. Li, G. Liu, B. Liu, Z. Min, D. Qian, J. Jiang and J. Li, *Electrochim. Acta*, 2018, **265**, 577-585.
12. M. Gong, Y. Li, H. Wang, Y. Liang, J. Z. Wu, J. Zhou, J. Wang, T. Regier, F. Wei and H. Dai, *J. Am. Chem. Soc.*, 2013, **135**, 8452-8455.
13. H. Jin, S. Mao, G. Zhan, F. Xu, X. Bao and Y. Wang, *J. Mater. Chem. A*, 2017, **5**, 1078-1084.
14. S. Fu, J. Song, C. Zhu, G.-L. Xu, K. Amine, C. Sun, X. Li, M. H. Engelhard, D. Du and Y. Lin, *Nano Energy*, 2018, **44**, 319-326.
15. D. T. Tran, H. T. Le, V. H. Hoa, N. H. Kim and J. H. Lee, *Nano Energy*, 2021, **84**, 105861.
16. W. Cai, R. Chen, H. Yang, H. B. Tao, H.-Y. Wang, J. Gao, W. Liu, S. Liu, S.-F. Hung and B. Liu, *Nano Lett.*, 2020, **20**, 4278-4285.
17. J. Chen, Q. Long, K. Xiao, T. Ouyang, N. Li, S. Ye and Z.-Q. Liu, *Sci. Bull.*, 2021, **66**, 1063-1072.